LAWRENCE
LIVERMORE
NATIONAL
LABORATORY

LLNL-JRNL-413891

X-Ray wave-front analysis and phase reconstruction with a two-dimensional shearing interferometer

K. Baker

June 15, 2009

Optical Engineering

Disclaimer

X-Ray wave-front analysis and phase reconstruction with a two-dimensional shearing interferometer

K.L. Baker*

Lawrence Livermore National Laboratory, 7000 East Ave., L-210 Livermore, CA, 94550 USA

Corresponding author: baker7@llnl.gov

This article presents the design and simulations of the expected performance of a novel two-dimensional x-ray shearing interferometer. This interferometer uses crossed phase gratings in a single plane and is capable of operation over a wide range of energies extending from several hundred eV to tens of keV by varying the grating material and thickness. This interferometer is insensitive to vibrations and, unlike Moire′ deflectometers implemented in the hard x-ray regime, recovers the full two-dimensional phase profile of the x-ray beam rather than the gradient in only one dimension.

OCIS codes: *010.7350, 120.5050, 340.0340*.

1. INTRODUCTION

A number of interferometers have been implemented in the hard x-ray regime to measure either the phase or the gradient of the phase in the case shear interferometers and Moire′ deflectometers. The first hard x-ray interferometer implementation used three partially transmitting Bragg crystals and was manufactured from a highly pure single silicon crystal to minimize vibrational effects [1]. More recently a one-dimensional shear interferometer based on Lloyd's mirror has also been demonstrated [2]. Additionally, several instruments based on the principles of Moire′ deflectometery have been realized which measure the one-dimensional gradient in the hard x-ray wave-front [3,4]. These latter instruments are far less susceptible to vibrations than the phase-measuring interferometers or the one-dimensional shear interferometer based on a Lloyd's mirror. These latter instruments, as implemented however, can only measure the one-dimensional gradient of the phase and as such require multiple measurements with the grating rotated between measurements to determine the orthogonal gradients required to reconstruct the wave-front.

In this article a two-dimensional shearing interferometer, based on two orthogonal phase gratings, is introduced which can measure the two-dimensional wave-front gradient in the hard x-ray regime. This instrument measures the two-dimensional wave-front gradient in a single measurement and does not require multiple measurements or movement of the grating structure. The two-dimensional grating can be made on a single membrane or cut from a single thin film, making it insensitive to both vibrations and alignment. A two-dimensional shearing interferometer based on crossed phase gratings

has been implemented previously in the visible regime [5]. In this case the crossed phase gratings were formed by etching a chess board pattern into glass.

2. DESIGN of the ORTHOGONAL PHASE GRATING for the SHEARING INTERFEROMETER

The essential component in this two-dimensional shearing interferometer is a crossed phase grating which produces intensity spots on a detector whose relative shifts determine the local two-dimensional wave-front gradient. When a periodic structure is placed in a beam, images of that structure will appear downstream of the object as discovered by Talbot [6]. More precisely if a phase grating is placed in the beam composed of alternating equal width bars of 0 and π phases, then the field at the location of the phase structure will be reproduced a distance $d_T = d^2/2\lambda$ downstream of the phase structure. In this expression, d_T is the Talbot distance, d represents the pitch of the phase grating and λ is the wavelength of the source. At a distance equal to $d_T/4$ and $3d_T/4$, the initial phase pattern across the beam has become uniform and the initially uniform intensity has acquired the periodic structure of the initial phase pattern with the pitch of the intensity pattern equal to half that of the original phase grating. At a distance of $d_T/2$, the phase pattern is reversed from the original phase grating and the intensity pattern is uniform such that this particular location can not be used for wave-front sensing. In practice, the intensity pattern has well defined spots for propagation distances between $d_T/16$ and $7d_T/16$ and between $9d_T/16$ and $15d_T/16$. The two applications simulated below were performed at a distance of $\sim d_T/13$ where the intensity pattern from the initial phase profile has produced well defined spots.

Each of the two orthogonal gratings is designed such that the even orders of the grating are eliminated. In order for the efficiency of the even orders, greater than the m=0 order, of a transmission grating to go to zero at x-ray wavelengths, the width of the slits must be half of the grating pitch [7,8]. In addition for the efficiency of the m=0 order of the grating to go to zero, there must be negligible absorption and the bar structure of the grating must produce a shift of π radians relative to the slits of the grating [7,8]. At x-ray wavelengths the index of refraction is expressed as $n = (1-\delta)+i\beta$, where $1-\delta$ gives rise to a phase shift as the x-rays pass through the sample and the β term results in absorption. The length for a π phase shift, x_π, can be expressed as $x_\pi = \lambda/(2\delta)$ and the absorption length, x_μ, can be written as $x_\mu = \lambda/(4\pi\beta)$. Fig. 1 represents the attenuation and π phase shift lengths for several elements as a function of x-ray energy. As can be seen in Fig. 1, the light elements can easily be made to provide the desired π phase shift and yet not provide any significant absorption of the x rays. As a specific example we take Carbon and go through the design for a 5 keV phase grating. For this example the width of the bar structure in the grating is identical to that of the slits such that all even orders above m=0 go to zero. The Carbon bars are made with a thickness of 6.74 μm such that a π phase shift is achieved for 5 keV x rays and the efficiency of the m=0 order approaches zero. The order efficiency as a function of x-ray energy for this grating is then shown in Fig. 2. At the design energy of 5 keV, the efficiency of the m=0 order approaches zero and the efficiency of the $m = \pm 1$ order is approximately 40 %. The efficiency of the odd orders goes approximately as $1/m^2$ with the $m=\pm 3$ and ± 5 shown in Fig. 2 [7,8].

3. SIMULATED PERFORMANCE of the 2-D X-RAY SHEARING INTERFEROMETER

Two applications of the shearing interferometer are presented below, both tailored to the next generation of hard x-ray free electron lasers such as the Linac Coherent Light Source(LCLS) [9], the Spring-8 Compact SASE Source(SCSS) [10], and the European X-Ray Free Electron Laser(Euro XFEL) [11]. The LCLS source will have a high transverse coherence, ~80%, a narrow bandwidth, $\Delta E/E \sim 0.1\%$, and operate over a range of x-ray energies, 0.8 to 8 keV in the fundamental. In both simulations, an x-ray energy of 0.8 keV was assumed with an x-ray beam diverging with an f/# of 3000, where the f/# is defined as the diameter of the focal length of the focusing optic divided by the diameter of the x-ray beam. The phase gratings were simulated with bar and slit widths equal to 12.5 μm, thus producing 80 spots across the detector which was located 15 mm past the plane containing the orthogonal phase gratings. The first application presented involves measuring the electric field at the shearing interferometer and then propagating this field back to focus to determine the far-field intensity pattern of the x-ray beam. The second application involves placing a phase object half way between the x-ray focus and the crossed phase gratings and determining the phase of the object based on the field measurement by the shearing interferometer. The latter example assumes the wave-front of the x-ray source is reproducible. The geometry of both simulations is shown in Fig. 3 below. In the former application there is no phase object placed in the beam. In both simulations the two orthogonal phase gratings are placed 3 meters from the focus of the x-ray source where the beam has expanded to a diameter is 1 mm. In both of these applications there is a significant focus term to the phase which must be accurately

recovered in order to recover the phase of an object placed in the beam or the residual aberrations in the beam itself. These simulations used an iterative reconstruction technique to accurately recover the small phase perturbations within the large focus term.

The iterative reconstruction process is very similar to a closed-loop adaptive optics system. In a typical closed-loop adaptive optics application, an initial electric-field defined by a phase and amplitude enters an optical system and is relay imaged onto a deformable mirror and subsequently onto a wave-front sensor. In the case of a two-dimensional shearing interferometer wave-front sensor, a two-dimensional grating would be used to form spots on the wave-front sensor camera. The difference between the locations of these spots and a set of reference spots, generated when a nearly perfect wave-front enters the system, is used to determine the local gradients in the wave-front. The wave-front is then reconstructed from these local gradients. Through the use of a gain factor, a percentage of the calculated wave-front is used to change the shape of the deformable mirror such that the measured spots from subsequent measurements of the electric field approach the reference spot locations and hence the wave-front approaches a nearly perfect wave-front.

A flow chart of the algorithm used in the simulations below is shown in Figure 4. The primary difference between the closed-loop application described above and the iterative reconstruction process is that rather than driving the solution to reference centroid locations with the use of a deformable mirror, the phase is driven to the initial measured centroid locations using a simulation loop. This is accomplished numerically by using the reconstructed phase to form simulated shearing interferometer spots on a simulated wave-front sensor camera and then comparing the numerically formed spots to

the initial measured spots. The gradients are then calculated from the differences between the simulated spot locations and the measured spot locations. Although the initial measured spots contain detector noise, no noise is added to the simulated shearing interferometer spots. The wave-front is reconstructed from these gradients and a numeric gain factor is used to add a percentage of the reconstructed wave-front to the composite wave-front from the previous iterations. In this approach the simulated shearing interferometer spot locations are driven towards the measured spot locations and hence the reconstructed wave-front is driven to the initial wave-front being measured. Using this technique errors in the boundary conditions can be significantly reduced and large aberrations can be reconstructed with very low phase variance between the initial phase and the reconstructed phase as shown in the following two sections.

Both simulations discussed below utilize wave optics simulations to transport the electric field between the various planes. The grating structure and the phase object are added to the electric field after the field has been propagated to their respective location. The wave-front is reconstructed from the simulated spots by first locating the displacement of each of the spots with a center-of-mass centroider and then reconstructing the resulting gradients with a multigrid wave-front reconstructor [12,13].

A. Reconstruction of the far-field intensity pattern

The first application is motivated by the desire to know the far-field intensity pattern that is being used to scatter off molecules in an attempt to characterize the structure of protein molecules that are not easily grown as crystals. The protein structure is determined by measuring the diffraction pattern from single molecules many times to build up all orientations of the molecules and then through tomographic reconstruction techniques to

recover the protein's three-dimensional structure. In this case the x-ray beam is focused and the shearing interferometer is placed 3 meters downstream of focus. The beam propagates 15 mm past the phase gratings where the resultant spots are formed on the detector. The intensity of the spots provide the local intensity of the field and the displacement of the spots determines the phase of the field at the phase gratings. The reconstructed field is then propagated back to focus to recover the far-field pattern of the x-ray beam. For this application an initial phase aberration was placed on the x-ray beam as shown in Fig. 5a below. The resultant far-field pattern with that phase aberration is shown in Fig. 5b. After the phase of the beam has been determined by reconstructing the local gradients from the spot displacements, the field is back-propagated to focus where the far-field intensity pattern is formed as shown in Fig. 5c.

B. Reconstruction of a phase object

The second application involves using an x-ray source to determine the phase of an unknown object placed in the beam. This application is also done with an expanding beam which is much more difficult than a collimated beam due to the large focus term which dominates the phase measurement. In this case a star-shaped phase object is placed midway between the focus of the x-ray beam and the crossed phase gratings. Fig. 6a and 6b represents the intensity pattern at the crossed phase gratings and 15 mm past the crossed phase gratings, respectively, with no phase object in the beam. Fig. 6c and 6d represents the intensity pattern at the crossed phase gratings and 15 mm past the crossed phase gratings, respectively, with the star-shaped phase object in the beam as shown in Fig. 7a. Based on the spot patterns in Fig. 6b and 6d, the local gradients are determined,

the phase reconstructed, the amplitude solved for and the fields at the entrance to the crossed phase gratings determined. The resultant fields are then back-propagated to the location where the phase object was placed in the beam. The two phases are then subtracted and the resultant phase unwrapped using a multigrid algorithm [13] to determine the phase of the object. The results of this phase recovery process are shown in Fig. 7b below. Fig. 7c shows an azimuthal lineout at a radius of one fourth the object's diameter for both the actual, black line, and reconstructed phases, dashed gray line, in Fig. 7a and 7b respectively. This lineout illustrates that the amplitude and spatial frequency of the phase object are quantitatively reproduced. There is a slight high frequency degradation as evidenced by the slope of the edges in the reconstructed phase vs. the actual phase and a low frequency noise term present in the reconstructed phase. The mean error in the full-width-at-half-maximum and the amplitude between the reconstructed vs. applied phase bars shown in Fig. 7c was 13 % and 0.4 %, respectively.

ACKNOWLEDGMENTS

This work was performed under the auspices of the U.S. Department of Energy by Lawrence Livermore National Laboratory in part under Contract W-7405-Eng-48 and in part under Contract DE-AC52-07NA27344.

REFERENCES

1. U. Bonse, and M. Hart, "An X-Ray Interferometer," Appl. Phys. Lett. **6**, 155 (1965).
2. W. Cash, et al., "Laboratory detection of X-ray fringes with a grazing-incidence interferometer," Nature **407**, 160 (2000).
3. C. David, et al., "Differential x-ray phase contrast imaging using a shearing interferometer," Appl. Phys. Lett. **81**, 3287 (2002).
4. T. Weitkamp, et al., "X-ray wavefront analysis and optics characterization with a grating interferometer," Appl. Phys. Lett. **86**, 054101 (2005).
5. J. Primot and N. Guerineau, "Extended Hartmann test based on the psuedoguiding property of a Hartmann mask completed by a phase chessboard," Appl. Opt. **39**, 5715 (2000).
6. F. Talbot, "Facts relating to optical science IV,"Philos. Mag. **9**, 401 (1836).
7. H.W. Schnopper, et al., "Diffraction grating transmission efficiencies for XUV and soft x rays," Appl. Opt. **16**, 1088 (1977).
8. M.C. Hettrick, et al., "Profiled bar transmission gratings: soft-x-ray calibration of new Kirchoff solutions," Appl. Opt. **43**, 3772 (2004).
9. *Linac Coherent Light Source (LCLS) Design Study Report,*. 1998: National Technical Information Services, 5285 Port Royal Road, Springfield, Virginia, 22161.
10. T. Shintake, et al., "Status of SPring-8 compact SASE source FEL project," Nucl. Inst. and Meth. **A507**, 382 (2003).
11. M. Altarelli et al. (eds.), *XFEL Technical Design*. August 2006., DESY: Hamburg.
12. K.L. Baker and M.M Moallem, "Iteratively Weighted Centroiding for Shack-Hartmann Wave-front Sensors," Optics Express **15**, 5147 (2007).

13. K. L. Baker, “Least-Squares Wave-Front Reconstruction of Shack-Hartmann Sensors and Shearing Interferometers using Multigrid Techniques,” Rev. Scien. Instr. **76**, 053502 (2005).

FIGURE CAPTIONS

Figure 1 Attenuation and π phase shift lengths for several elements as a function of x-ray energy.

Figure 2 Spectral order efficiency for a transmission grating composed of 6.74 μm thick Carbon bars. This thickness provides the required pi phase shift at 5 keV such that the zero order of the grating approaches zero.

Figure 3 Simulation geometry used in both reconstructing the far-field and also in retrieving the phase of an object placed in the x-ray beam.

Figure 4 Flowchart for the open-loop iterative application.

Figure 5 Reconstructed far-field spot using the shearing interferometer.

Figure 6 Intensity profiles at the entrance and 15 mm after having passes through a two-dimensional crossed phase grating.

Figure 7 Retrieved phase object. Fig. 6a shows the actual phase of the object placed in the expanding x-ray beam and Fig. 6b shows the reconstructed phase. Fig. 6c shows an azimuthal lineout through the two phases at a radius of one fourth the object's diameter.

FIGURES

KL Baker

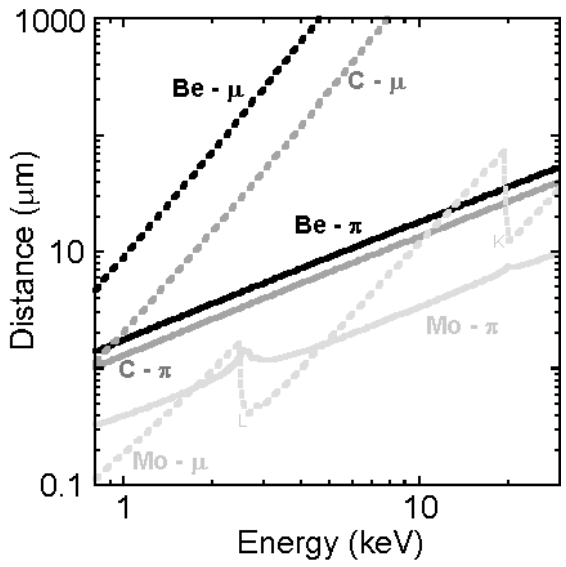

Figure 1

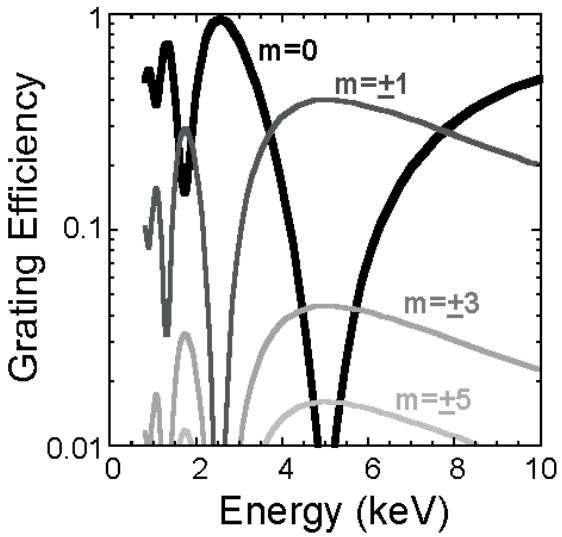

Figure 2

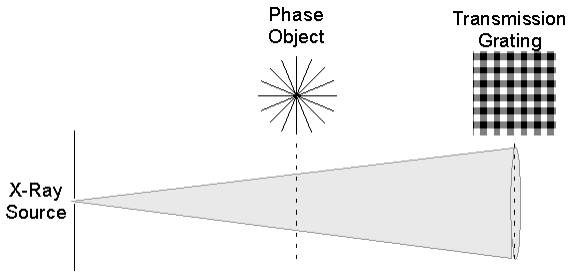

Figure 3

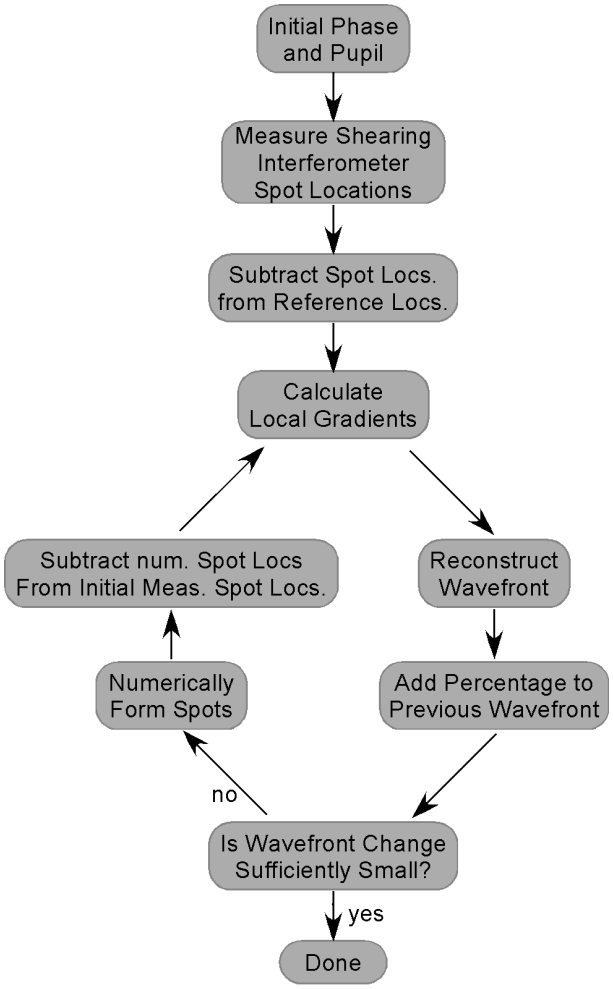
Initial Phase and Pupil
Measure Shearing Interferometer Spot Locations
Subtract Spot Locs. from Reference Locs.
Calculate Local Gradients
Subtract num. Spot Locs From Initial Meas. Spot Locs.
Reconstruct Wavefront
Numerically Form Spots
Add Percentage to Previous Wavefront
no
Is Wavefront Change Sufficiently Small?
yes
Done

Figure 4

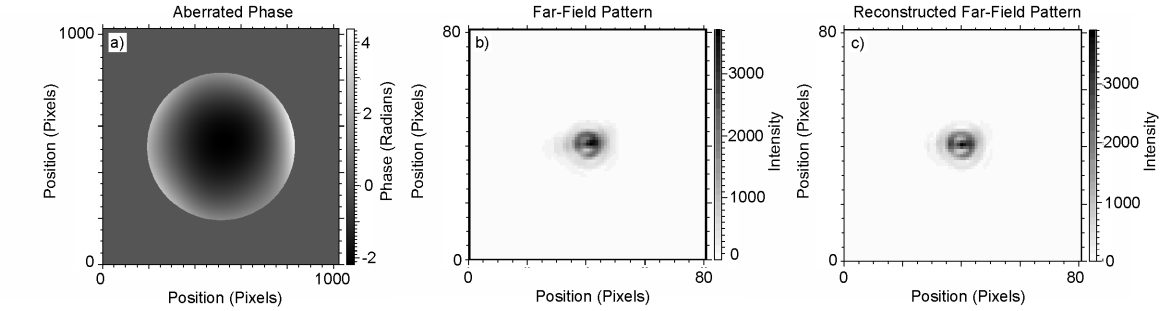
Aberrated Phase
a)
1000
0
Position (Pixels)
0
1000
Position (Pixels)
4
2
0
-2
Phase (Radians)
Far-Field Pattern
b)
80
0
Position (Pixels)
0
80
Position (Pixels)
3000
2000
1000
0
Intensity
Reconstructed Far-Field Pattern
c)
80
0
Position (Pixels)
0
80
Position (Pixels)
3000
2000
1000
0
Intensity

Figure 5

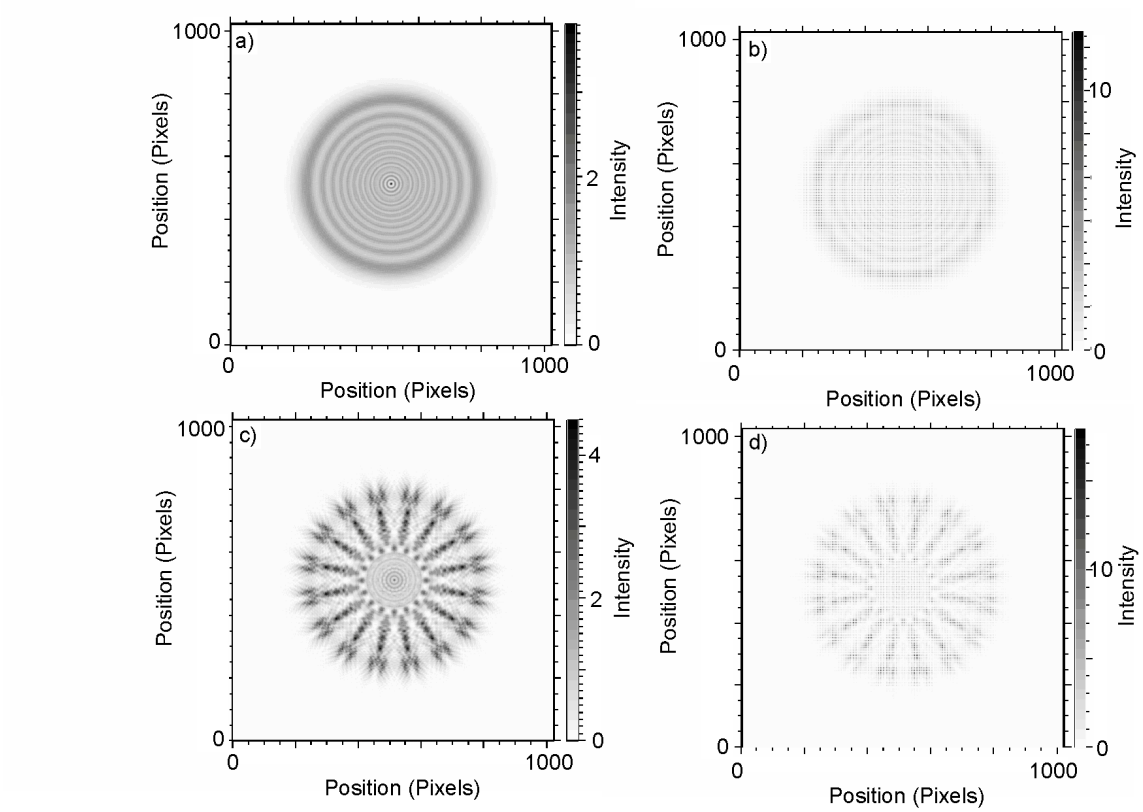

Figure 6

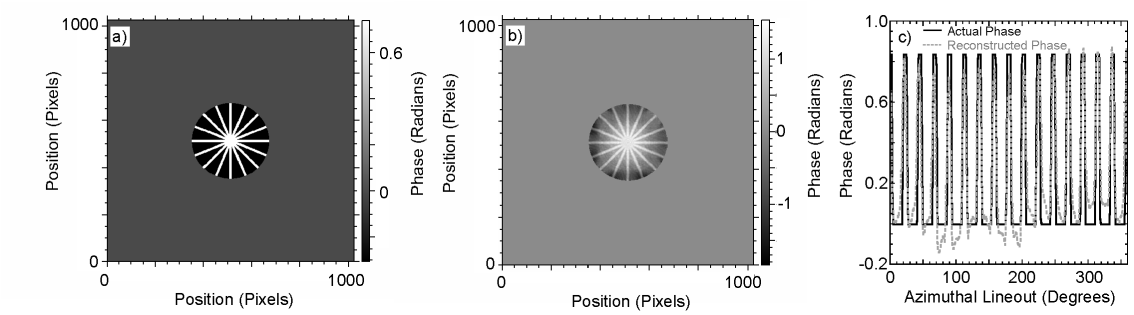
a)
1000
0
0
1000
Position (Pixels)
Position (Pixels)
0.6
0
Phase (Radians)
b)
1000
0
0
1000
Position (Pixels)
Position (Pixels)
1
0
-1
Phase (Radians)
c)
Actual Phase
Reconstructed Phase
1.0
0.6
0.2
-0.2
0
100
200
300
Azimuthal Lineout (Degrees)
Phase (Radians)

Figure 7